ELSEVIER

Materials Science and Engineering B 141 (2007) 55–60

ENGINEERING B

www.elsevier.com/locate/mseb

Oxygen permeability and improved stability of a permeable Zr-substituted perovskite membrane for air separation

Hui Lu [1], You Cong, Weishen Yang *

State Key Laboratory of Catalysis, Dalian Institute of Chemical Physics, Chinese Academy of Sciences, P.O. Box 110, Dalian 116023, PR China

Received 5 February 2007; received in revised form 15 April 2007; accepted 26 May 2007

Abstract

Zr-substituted $Ba_{0.5}Sr_{0.5}Co_{0.8}Fe_{0.1}Zr_{0.1}O_{3-\delta}$ (BSCFZO) powders for oxygen membrane were synthesized by the solid-state reaction (SSR) method. Oxygen permeation fluxes (J_{O_2}) across the dense $Ba_{0.5}Sr_{0.5}Co_{0.8}Fe_{0.2}O_{3-\delta}$ (BSCFO) and BSCFZO membrane disks were measured at 973–1123 K, and they increased as BSCFO (synthesized by improved EDTA–citric acid complexing method, ECC) > BSCFO (SSR) > BSCFZO. The reduced oxygen permeability of Zr-substituting BSCFZO material can be attributed primarily to the higher oxidation state of Zr cations than ones of iron cations, thus lead to the decrease in the oxygen vacancy concentration in BSCFO. Oxygen permeation measurements with different oxygen partial pressure gradients and membrane thicknesses demonstrate the bulk oxide ionic diffusion is the rate-limiting step for the BSCFZO membrane in the range of temperatures investigated (973–1123 K). The enhanced stability of BSCFZO demonstrated by the differential thermal analysis (DTA) and high-temperature X-ray diffraction (HT-XRD) characterizations, show that the structural stability can be improved when the Fe ions in the B-sites of BSCFO materials are substituted partially by Zr cations.

Keywords: Perovskite; Oxygen-permeable membrane; Oxygen permeability; Stability

1. Introduction

Oxygen-deficient perovskite-type oxides (ABO_3) are of interest for practical applications in solid oxide fuel cell, oxygen sensor, and as oxygen-permeable membranes for oxygen separation at elevated temperatures [1–8], especially as membrane reactors for the selective oxidation of light hydrocarbons [1,4,7,8]. Along with predominantly electronic conductivity, these perovskite oxides exhibit high oxygen ionic conduction, which often is greater than that in the solid electrolytes of the stabilized ZrO_2 or doped CeO_2 [1]. The family of perovskite-type $SrCo_{1-x}Fe_xO_{3-\delta}$ had been demonstrated to possess excellent ionic conduction and oxygen permeability by many researchers [1,3,7–12]. As one of the typical perovskite membrane materials, $SrCo_{0.8}Fe_{0.2}O_{3-\delta}$ (SCFO), which possesses attractive oxygen permeability, the physicochemical properties for it, such as the surface exchange kinetics, the electronic/oxide ionic conductivities, the oxygen nonstoichiometry and structural stability, as well as the oxygen permeation and its mechanism, had been studied extensively [1,3,9,10]. Unfortunately, the poor chemical and structural stability (possible phase decomposition, segregation or transformation) of SCFO in the reduced environment limited its potential applications. In addition, SCFO material possess some other disadvantages, such as the extremely high thermal expansion coefficients and the insufficient mechanical strength, which further enable it to be improper as separation membranes for oxygen separation and/or membrane reactors for partial oxidation of light alkanes [1,3,8–12].

In order to overcome those disadvantages of SCFO mentioned above, extensive work had been performed on it [1,6,8,9–13]. Based on the SCFO material, $Ba_{0.5}Sr_{0.5}Co_{0.8}Fe_{0.2}O_{3-\delta}$ (BSCFO) perovskite-type material synthesized by the improved EDTA–citric acid complexing method, exhibits good oxygen permeability and permeation stability performance [8,11–13]. Through the proper substitution of Sr^{2+} in SCFO by the Ba^{2+} with a larger ionic radius, its structural stability was improved, and the oxygen permeability and its stability were also increased. However, the structural and oxygen permeation stability of the BSCFO membrane was still not good at the temperatures lower than 1123 K [11].

* Corresponding author. Tel.: +86 411 84379073; fax: +86 411 84694447.
E-mail address: yangws@dicp.ac.cn (W. Yang).
[1] Current address: Max-Planck-Institute for Dynamics of Complex Technical Systems, Max-Planck-Society, Sandtorstrasse 1, D-39106 Magdeburg, Germany.

0921-5107/$ – see front matter © 2007 Elsevier B.V. All rights reserved.
doi:10.1016/j.mseb.2007.05.006

We had developed some novel membrane materials with improved oxygen permeability and structural stability, which could be applied as oxygen-separation membranes or membrane reactors for the selective oxidation of light hydrocarbons [6,8,11–13]. The interests for Zr-substituted system are associated with the possible improvement of the mechanic, structural and stable performance of $SrCo(Fe)O_{3-\delta}$ ceramics, which can be achieved by the partial substitution of Fe ions with Zr^{4+} [14]. In this paper, Zr-substituted $Ba_{0.5}Sr_{0.5}Co_{0.8}Fe_{0.1}Zr_{0.1}O_{3-\delta}$ membrane materials were synthesized. Furthermore, the crystal structure, oxygen permeation, as well as structural stability of $Ba_{0.5}Sr_{0.5}Co_{0.8}Fe_{0.1}Zr_{0.1}O_{3-\delta}$ membranes were studied.

2. Experimental

2.1. Preparation of powders and membranes

The oxide powders of $Ba_{0.5}Sr_{0.5}Co_{0.8}Fe_{0.2}O_{3-\delta}$ (designated as BSCFO) and $Ba_{0.5}Sr_{0.5}Co_{0.8}Fe_{0.1}Zr_{0.1}O_{3-\delta}$ (designated as BSCFZO) oxygen-permeable membranes were synthesized by the solid-state reaction (SSR) method. The analytical reagents of $BaCO_3$, $SrCO_3$, Co_2O_3, Fe_2O_3 and ZrO_2 were used as the starting materials. Weighted in the aimed stoichiometry, they were mixed and milled well, and calcined at different temperatures (1123–1323 K) for 10 h with several intermediate grindings, and then the final oxide powders were obtained. As for BSCFO, the improved EDTA–citric acid complexing (ECC) method was also used, and the synthesis details were presented in previous references [11–13]. The calcined powders were dry-pressed at 15–20 MPa into pellets with diameter 16–17 mm, thickness 1–2 mm. The green disks were sintered by using heating rate 1–2 K/min to 1423–1473 K, holding for 3–10 h, and then cool down with the same rate to room temperature. These membranes were dense sintering bodies with closed pores as verified by gas testing, and the relative densities of ~91% were obtained for these membrane disks.

2.2. Characterizations

The crystal structure of the synthesized powders and sintered membranes were characterized by X-ray diffraction (XRD, Miniflex, Rigaku, Japan, using the Cu Kα radiation, 0.1542 nm). The high-temperature XRD (HT-XRD) experiments were performed in air by using a RINT D/MAX-2500/PC XRD instrument (Cu Kα Rigaku, Japan) equipped with a Rigaku PTC-30 heating unit. The HT-XRD output power was 40 kV × 100 mA, and the heating rate of the sample was 5 K/min. The temperature was held constant from the room temperature to 1373 K with an accuracy of about ±1 K.

Differential thermal analysis (DTA) was carried out at a scan rate of 10 K/min by using TG/DTA system (Perkin-Elmer, Pyris-Diamond). Samples in platinum boats, were measured with respect to an aluminum oxide reference.

2.3. Oxygen permeation measurements

Fig. 1 presents the configuration of high-temperature permeator unit for oxygen permeation measurements. Two kinds of special sealants were used as the high-temperature binding agents to seal the disc onto the stainless steel tube B (SS-B), and the side wall of the membrane disc was also covered with the paste to avoid the radial contribution to the oxygen permeation. The leakage was below 5% for all determinations, and all the calculated oxygen permeation fluxes (J_{O_2}) were corrected based on the measured leakage. Oxygen partial pressure difference across the membrane disks was established by using air on

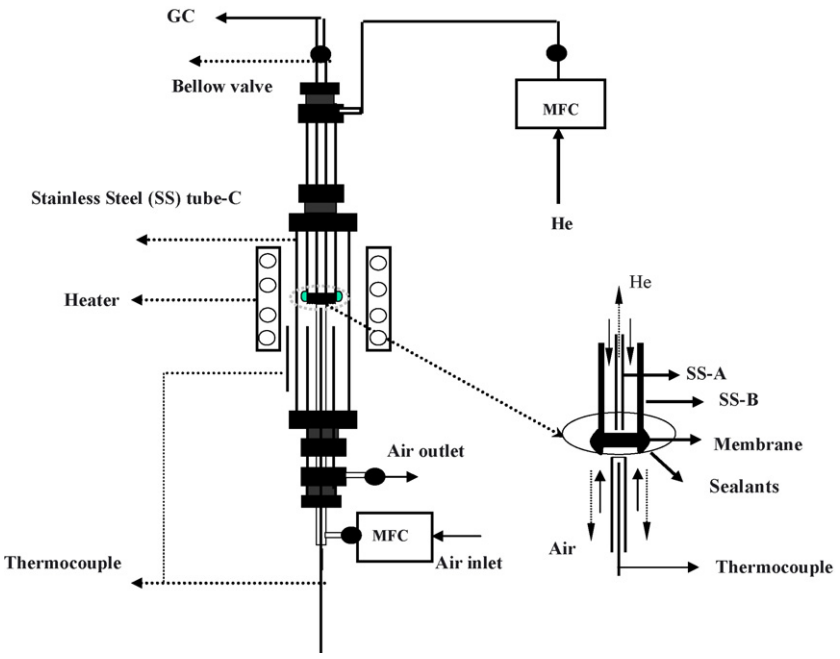

Fig. 1. Setup of the high-temperature permeator for oxygen permeation measurements.

the primary side and pure helium (He) gas on the secondary permeable side at atmospheric pressure. The air flow rate was kept at 150 ml/min on the primary side (sweep side, oxygen partial pressure: 0.21 atm), and He as sweep gas flow rates were in the range of 20–80 ml/min on the opposite side (permeation side, oxygen partial pressure varying on He flow rate). The oxygen permeation fluxes were calculated from O_2 concentration in the effluents of the permeated side of membrane disk by gas chromatography (GC, Agilent 6890 *Plus*, equipped with TCD and a 13× molecule sieve column for O_2 and possibly leaked N_2 separation) analysis. The details about the oxygen permeation measurements for the dense membrane disks were described previously [6,11,12].

3. Results and discussion

Fig. 2 shows the room temperature XRD patterns of the sintered BSCFO and BSCFZO membranes. It can be seen that the purely cubic perovskite-type structures were observed for both sintered BSCFO membrane disks synthesized by ECC and SSR methods (as shown in Fig. 2). While for BSCFZO material (Fig. 2c), minor impurities phase (Ba,Sr)ZrO_3 was found. Meanwhile, the expansion of lattice parameter ($a = 0.3989$ nm) of the cubic perovskite was observed due to the dissolution of larger ionic radius Zr^{4+} ($r = 186$ pm) ions in the B sites of BSCFO perovskite-type structure [14–16]. It was also reported that the solid solubility of ZrO_2 in the B-sites of $La_{0.7}Sr_{0.3}MnO_3$ (LSM) lattice occurred when exposed to Y_2O_3-stabilized ZrO_2 (YSZ), which resulted in the lattice expansion of LSM [17]. For BSCFO sample fabricated by SSR method, the lattice parameter (a) is 0.3977 nm, which is in agreement with that of BSCFO prepared by ECC method [11]. The lattice parameter of BSCFO is larger than that of SCFO ($a = 0.3863$ nm), and it might be due to the larger ion size of Ba^{2+} (175 pm) than that (158 pm) of Sr^{2+}.

Fig. 3 shows the oxygen permeation fluxes (J_{O_2}) of the dense BSCFO and BSCFZO membrane disks synthesized by SSR

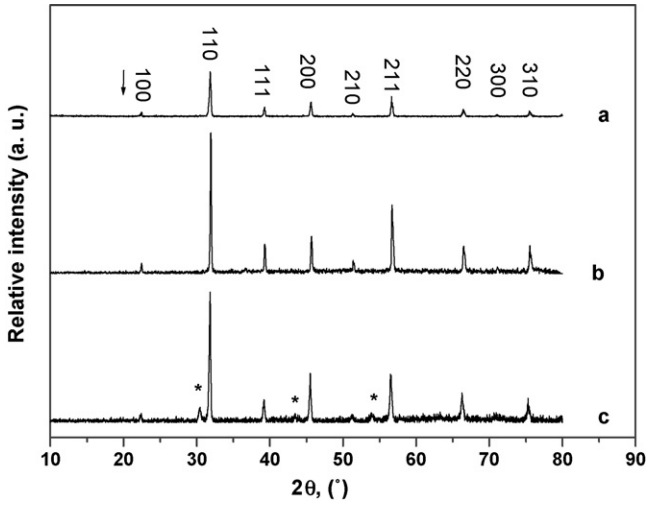

Fig. 2. XRD patterns of BSCFO and BSCFZO membranes: (a) BSCFO-ECC; (b) BSCFO-SSR and (c) BSCFZO. *, impurity (Ba,Sr)ZrO_3.

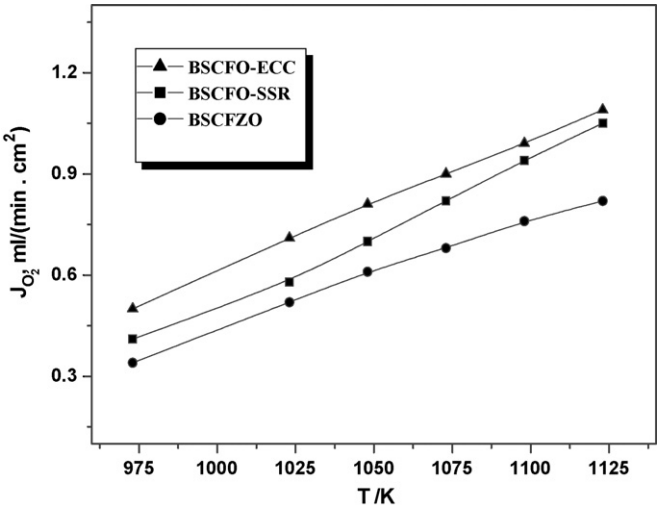

Fig. 3. Oxygen permeation fluxes of BSCFO and BSCFZO membranes disks at 973–1123 K, membrane thickness L: 1.46 mm.

method at 973–1123 K. For comparison, the oxygen permeation fluxes of BSCFO synthesized by ECC method are also presented. As for BSCFO membrane disk prepared by SSR method, the oxygen permeation fluxes could be reached 0.41 ml/(min cm^2) at 973 K, and 1.05 ml/(min cm^2) at 1123 K, respectively. These values are slightly lower than ones for BSCFO membrane synthesized by ECC method, 0.50 ml/(min cm^2) at 973 K and 1.09 ml/(min cm^2) at 1123 K, respectively. The preparation methods and sintering of membrane can influence on the physicochemical features of resultant membrane such as microstructure and crystallinity, and on the uniformity of local composition, possibly resulting in the difference of oxygen permeability [18–20]. In addition, these oxygen permeation results further demonstrated that BSCFO membrane possess excellent oxygen permeability.

Moreover, it can also be seen that the oxygen permeation fluxes of BSCFZO are lower than ones of BSCFO (as shown in Fig. 3). For the partially Zr-substituted BSCFZO material, Zr cations with relative higher ionic value state (4+) are incorporated into the B-sites of BSCFO perovskite structure, leading to the decrease in the oxygen vacancy concentration, just like $Ce^{3+/4+}$ (or $Cr^{3+/4+}$) as dopant [6,21,22]. In addition, Zr-incorporation into BSCFO can also increase the metal–oxygen (M–O) bonding energy and reduce the oxygen ionic conductivity, thus resulted in the lowered oxygen permeability. In the such case, oxygen anions near Zr^{4+} may be partially blocked and provides a minor contribution to the totally ionic transport [14]. The assumption could also be demonstrated based on the fact that oxygen ionic conduction in Cr-containing $SrCo_{0.9-x}Fe_{0.1}Cr_xO_{3-\delta}$ ($x = 0.01$–0.05) perovskites were lower than that in the parent compound, $SrCo_{0.9}Fe_{0.1}O_{3-\delta}$ [21,22]. Meanwhile, the impurities (Ba,Sr)ZrO_3 existing in perovskite BSCFZO may have certain contributions to the lowered oxygen permeability of BSCFZO membranes, which can block partly the oxygen ions transport route in the bulk and influence negatively on oxygen surface exchange kinetics at the membrane surfaces.

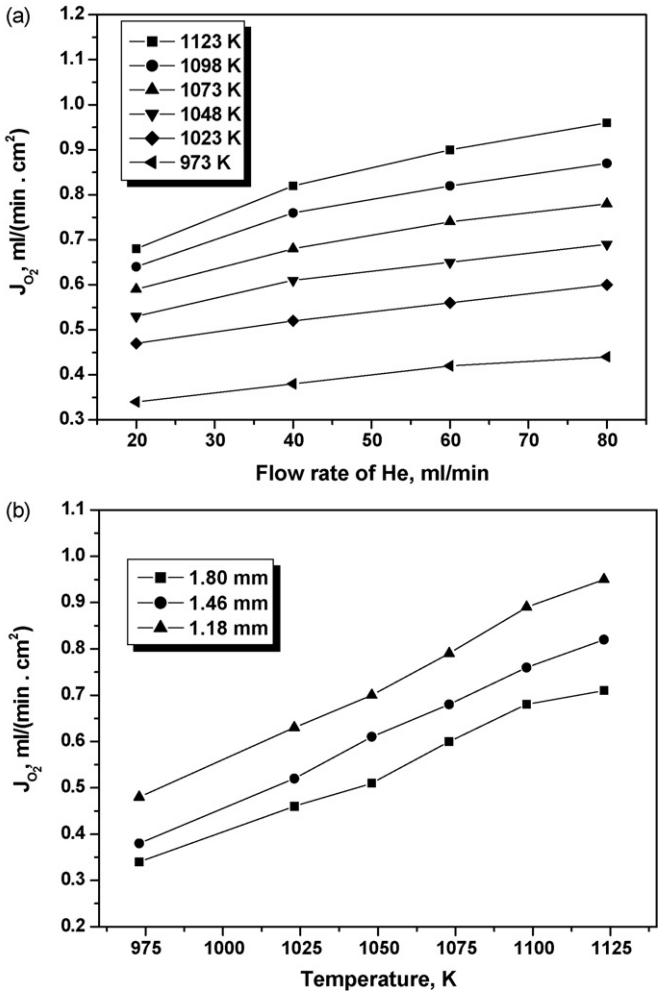

Fig. 4. Oxygen permeation fluxes of BSCFZO membranes with (a) sweep gas flow rate (L: 1.46 mm), and (b) membrane thickness (L), at 973–1123 K.

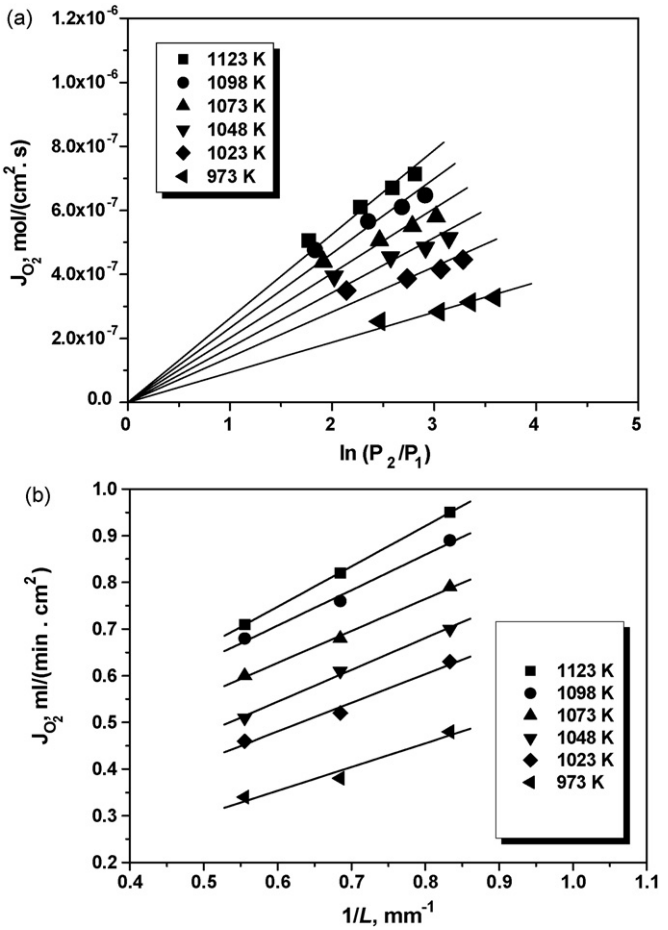

Fig. 5. Dependences of oxygen permeation flux of BSCFZO membrane on (a) oxygen partial pressure term, ln(P_2/P_1), and (b) membrane thickness (1/L), at 973–1123 K.

Fig. 4 presents the dependences of oxygen permeation fluxes of BSCFZO membranes on the sweep gas (He) flow rate and membrane thickness (L). It can be seen in Fig. 4a, the oxygen permeation flux was increased with the sweep gas flow. It is attributed to the higher oxygen partial gradient across the membrane as the sweep gas flow rate increases, and then result in the increasing of oxygen permeation flux of membrane, as expected. Moreover, it can also be seen that the oxygen permeation flux increased with decreasing membrane thickness in the range of temperature investigated (as shown in Fig. 4b).

For the dense mixed-conducting oxygen-permeable membrane, the bulk oxygen ionic diffusion and surface exchange kinetics steps are crucial for the whole oxygen transporting process [1,3–5,9,10]. According to the surface exchange current model suggested by Jacobson and co-workers [9,10], the oxygen permeation flux (J_{O_2}, mol s^{-1} cm^{-2}) is given by the following equation if the bulk oxygen ionic diffusion process is the rate-limiting step for oxygen permeation across the disk-type membrane:

$$J_{O_2} = \frac{C_i D_a}{4L} \ln\left(\frac{P_2}{P_1}\right) \quad (1)$$

where C_i (mol/cm^3) is the density of oxygen ions, D_a (cm^2/s) the ambipolar diffusion coefficient, L (cm) the thickness of membrane disk, P_1 (atm) and P_2 (atm) are the oxygen partial pressure for the low and high oxygen partial pressure sides across the membrane disk, respectively [9,10]. Eq. (1) predicts that, if the bulk oxide ionic diffusion process limits the oxygen permeation transport, the oxygen permeation fluxes should be proportional to the oxygen partial pressure gradients term ln(P_2/P_1), and to the reciprocal of the thickness (1/L) of the membrane disks. Fig. 5a shows the dependences of the oxygen permeation fluxes of BSCFZO membrane on pressure term ln(P_2/P_1), in the temperature range of 973–1123 K. It can be seen that linear relationships were obtained in the range of temperatures investigated. Fig. 5b also shows the oxygen permeation fluxes were basically proportional to the reciprocal of the membrane thickness (1/L). The results demonstrate that the bulk oxide ionic diffusion process is dominant across the BSCFZO membrane, and the contribution from the surface exchange kinetic steps may be poor or negligible to the overall rate-limiting process of oxygen permeation.

As for an oxygen-permeable membrane for practical applications, it is not enough to possess only excellent oxygen permeability, and the good stability of oxygen permeation is also

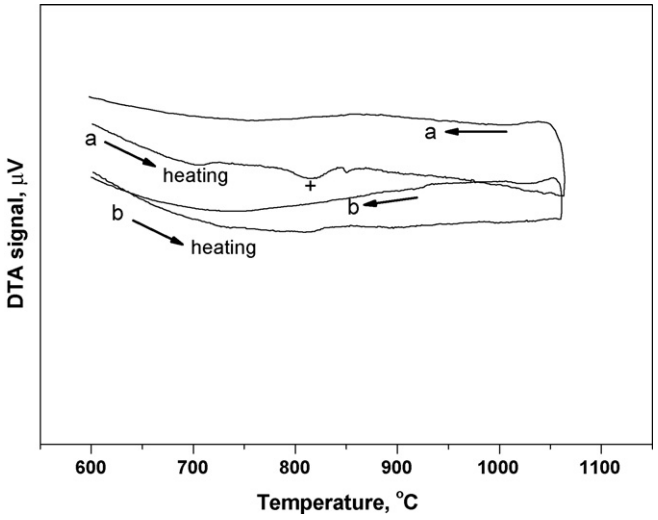

Fig. 6. DTA curves in the heating and cooling processes for BSCFO and BSCFZO: (a) BSCFO and (b) BSCFZO.

very crucial [1,3,11]. The BSCFZO membranes exhibit good stability of oxygen permeation even at lower temperature of 1023–1048 K. However, a decay in the oxygen permeation was found for BSCFO membranes at lower temperatures (<1123 K) [11,23]. The different phase compositions in the surface layer and the bulk demonstrated that surface segregation might be one reason for the oxygen permeation decay at reduced temperature (<1123 K). Meanwhile, the formation of carbonates on the membrane surface and the phase degradation/transformation possibly might be other important reasons [11,13,23]. The approximate stability limit of perovskite $SrCo_{0.9}Fe_{0.1}O_{3-\delta}$ doped by Cr ions was determined from the equilibration kinetics, and significantly improved phase stability could be obtained [21,22]. The improved stability of SCFO material may be attributed to the higher oxidation state of $Cr^{3+/4+}$ cations with respect to Fe ions because the presence of these higher oxidation ions in B-sites may stabilize neighboring octahedral oxygen resulting from stronger columbic attraction.

To elucidate the structural stability of BSCFO and BSCFZO materials, the DTA and HT-XRD were performed. The DTA curves of BSCFO and BSCFZO materials are shown in Fig. 6, and a small endothermic peak at 818 °C in heating process for BSCFO material was found. However, no obvious endothermic or exothermic peaks were observed for BSCFZO material in the heating and cooling processes. Furthermore, the high-temperature XRD experiments of BSCFO and BSCFZO powders were also conducted (as shown in Fig. 7). Two additionally unidentified diffraction peaks appeared when the temperature increased to 1073 K (Fig. 7a), indicating the occurrence of the partial phase decomposition/segregation or phase transformation of the cubic perovskite structure. Dassonneville et al. [24] also observed the similar phase changes phenomena in the BSCFO material, though the unidentified peaks were different from the results here. However, the cubic perovskite structure could be kept in the range of temperatures investigated except for the appearance of these two unidentified peaks, and no phase transition/transformation of cubic perovskite structure

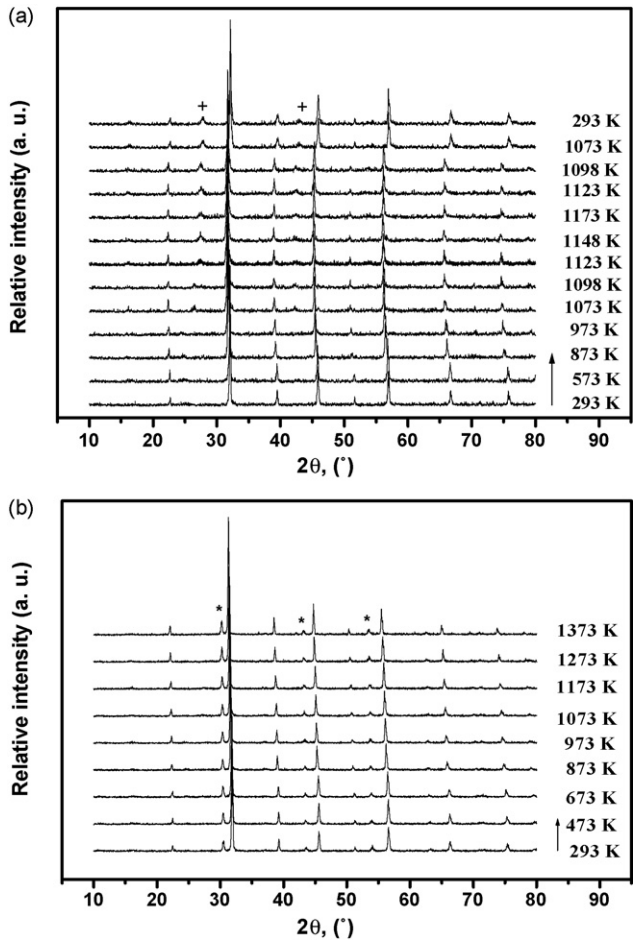

Fig. 7. High-temperature XRD patterns of BSCFO and BSCFZO: (a) BSCFO and (b) BSCFZO. *, impurity $(Ba,Sr)ZrO_3$ in BSCFZO; +, appeared unknown reflections in BSCFO; and the other unmarked reflections, cubic pervoskite.

were observed for BSCFO material. However, for cubic perovskite BSCFZO, the cubic perovskite and impurities phases were kept in BSCFZO material. There were not any other phase transformation/transition observed in the range of temperatures investigated (as shown in Fig. 7b), demonstrating the highly structural stability of the as-synthesized BSCFZO. The partial substitution of Fe ions in the B-sites of the perovskite-type structure parents by higher valence state ions (Zr^{4+}, Sn^{4+}, $Ce^{3+/4+}$ or $Cr^{3+/4+}$, etc.) can increase the M–O bonding energy, and then resulted in the enhanced structural stability [6,14,21,22]. For the practical application of BSCFO and its related materials either as oxygen-separation membranes or membrane reactors for catalytic oxidation of light hydrocarbons [3,8,24–36], or application as cathode in solid oxide fuel cells [2,37,38], the further studies would be necessary.

4. Conclusions

The oxygen-permeable $Ba_{0.5}Sr_{0.5}Co_{0.8}Fe_{0.2}O_{3-\delta}$ (BSCFO) and Zr-substituted $Ba_{0.5}Sr_{0.5}Co_{0.8}Fe_{0.1}Zr_{0.1}O_{3-\delta}$ (BSCFZO) membranes were synthesized by the solid-state reaction method. BSCFZO possess cubic perovskite structure, but minor $(Ba,Sr)ZrO_3$ impurity exists. The lattice parameter (a) of

BSCFZO was increased as compared with that of BSCFO, which is ascribed to the larger ionic radii of octahedral Zr^{4+} ions than that of Fe^{3+} ions. Oxygen permeation measurements of the dense BSCFO and BSCFZO membrane disks showed the oxygen permeability were increased in the order: BSCFO (ECC) > BSCFO (SSR) > BSCFZO. Moreover, oxygen permeation studies also demonstrated that the bulk oxide ionic diffusion process was the rate-limiting step for BSCFZO membrane in the range of temperatures investigated. The improved structural stability demonstrated by DTA and HT-XRD characterizations on BSCFZO membrane, which was resulted from the presence of Zr^{4+} in the B-sites of BSCFZO can stabilize the neighboring oxygen octahedral, and increase the metal–oxygen (M–O) bonding energy. Considering the good oxygen permeation and stability, BSCFZO should be an attractive material for practical applications as an oxygen-separation membrane or in membrane reactors for the catalytic conversion of light alkanes.

Acknowledgements

The authors gratefully acknowledge financial support from the National Nature Science Foundation of China (Grant No. 50332040), and the Ministry of Science and Technology, China (Grant No. 2005CB221404). We are also grateful to Dr. Jianhua Tong, Dr. Haihui Wang and Dr. Zengqiang Deng for valuable discussion with them.

References

[1] H.J.M. Bouwmeester, A.J. Burggraaf, in: A.J. Burggraaf, L. Cot (Eds.), Fundamentals of Inorganic Membrane Science and Technology, Elsevier, Amsterdam, 1996, p. 435.
[2] Z.P. Shao, S.M. Haile, Nature 431 (2004) 170.
[3] H.J.M. Bouwmeester, Catal. Today 82 (2003) 141.
[4] A. Thursfield, I.S. Metcalfe, J. Solid State Electrochem. 10 (2006) 604.
[5] B.C.H. Steele, Curr. Opin. Solid State Mater. Sci. 1 (1996) 684.
[6] X.F. Zhu, H.H. Wang, W.S. Yang, Chem. Commun. 9 (2004) 1130.
[7] Y. Zeng, Y.S. Lin, S.L. Swartz, J. Membr. Sci. 150 (1998) 87.
[8] H.H. Wang, Y. Cong, W.S. Yang, Chem. Commun. 14 (2002) 1468.
[9] L. Qiu, T.H. Lee, L.M. Liu, Y.L. Yang, A.J. Jacobson, Solid State Ionics 76 (1995) 321.
[10] S. Kim, Y.L. Yang, A.J. Jacobson, B. Abeles, Solid State Ionics 106 (1998) 189.
[11] Z.P. Shao, W.S. Yang, Y. Cong, H. Dong, J.H. Tong, G.X. Xiong, J. Membr. Sci. 172 (2000) 177.
[12] H. Lu, J.H. Tong, Y. Cong, W.S. Yang, Catal. Today 104 (2005) 154.
[13] W.S. Yang, H.H. Wang, X.F. Zhu, L.W. Lin, Top. Catal. 35 (2005) 155.
[14] L. Yang, X.H. Gu, L. Tan, L.X. Zhang, C.Q. Wang, N.P. Xu, Sep. Purif. Technol. 32 (2003) 301.
[15] R.D. Shannon, Acta Crystallogr. A 32 (1976) 751.
[16] H. Lu, Z.Q. Deng, J.H. Tong, W.S. Yang, Mater. Lett. 59 (2005) 2285.
[17] K. Wiik, C.R. Schmidt, S. Faaland, S. Shamsili, M.A. Einarsrud, T. Grande, J. Am. Ceram. Soc. 82 (1999) 721.
[18] V.V. Kharton, E.N. Naumovich, A.V. Kovalevsky, A.P. Viskup, F.M. Figueiredo, I.A. Bashmakov, F.M.B. Marques, Solid State Ionics 138 (2000) 135.
[19] A.L. Shaula, A.P. Viskup, V.V. Kharton, D.I. Logvinovich, E.N. Naumovich, J.R. Frade, F.M.B. Marques, Mater. Res. Bull. 38 (2003) 353.
[20] X. Qi, Y.S. Lin, S.L. Swartz, Ind. Eng. Chem. Res. 39 (2000) 646.
[21] V.V. Kharton, V.N. Tikhonovich, S.B. Li, E.N. Naumovich, A.V. Nikolaev, A.P. Viskup, I.A. Bashmakov, A.A. Yaremchenko, J. Electrochem. Soc. 145 (1998) 1363.
[22] V.N. Tikhonovich, O.M. Zharkovskaya, E.N. Naumovich, I.A. Bashmakov, V.V. Kharton, A.A. Vecher, Solid State Ionics 160 (2003) 259.
[23] Z.P. Shao, PhD Thesis, Dalian Institute of Chemical Physics, Chinese Academy of Sciences, Dalian, 2000.
[24] M.R. Dassonneville, S. Rosini, A.C. van Veen, D. Farrusseng, C. Mirodatos, Catal. Today 104 (2005) 131.
[25] H. Lu, J.H. Tong, Z.Q. Deng, Y. Cong, W.S. Yang, Mater. Res. Bull. 41 (2006) 683.
[26] A. Thursfield, I.S. Metcalfe, J. Mater. Chem. 14 (2004) 2475.
[27] H. Lu, Y. Cong, W.S. Yang, Solid State Ionics 177 (2006) 595.
[28] H. Dong, Z.P. Shao, G.X. Xiong, J.H. Tong, S.S. Sheng, W.S. Yang, Catal. Today 67 (2001) 3.
[29] H.H. Wang, Y. Cong, W.S. Yang, Catal. Today 104 (2005) 160.
[30] Z.P. Shao, G.X. Xiong, H. Dong, W.S. Yang, L.W. Lin, Sep. Purif. Technol. 25 (2001) 97.
[31] H.H. Wang, Y. Cong, W.S. Yang, J. Membr. Sci. 209 (2002) 143.
[32] L. Tan, X.H. Gu, L. Yang, W.Q. Jin, L.X. Zhang, N.P. Xu, J. Membr. Sci. 212 (2003) 157.
[33] C.S. Chen, S.J. Feng, S. Ran, D.C. Zhu, W. Liu, H.J.M. Bouwmeester, Angew. Chem. Int. Ed. 42 (2003) 5196.
[34] A.C. van Veen, M. Rebeilleau, D. Farrusseng, C. Mirodatos, Chem. Commun. 1 (2003) 32.
[35] J.H. Tong, W.S. Yang, H. Suda, K. Haraya, Catal. Today 118 (2006) 144.
[36] H.H. Wang, C. Tablet, A. Feldhoff, J. Caro, Adv. Mater. 17 (2005) 1785.
[37] Z.S. Duan, M. Yang, A.Y. Yan, Z.F. Hou, Y.L. Dong, Y. Cong, M.J. Cheng, W.S. Yang, J. Power Sources 160 (2006) 57.
[38] Q.L. Liu, K.A. Khor, S.H. Chan, J. Power Sources 161 (2006) 123.